

## Chapter

# Role of Carbon Nanotube for Flexible Supercapacitor Application

*Shalu Rani, Sanjay Kumar and Ritesh Bhardwaj*

## Abstract

In this current era, with the ever-increasing demand for portable and wearable energy storage devices, the supercapacitor (SC) plays a very positive role to fulfill this gap. Carbon nanotubes (CNTs) are extremely promising material candidate in flexible SC where it works as an electrode to enhance the energy and power densities of the SC because of their remarkable mechanical property, high electrical conductivity, large surface area, and ease to functionalize. Moreover, CNTs can assemble into various macroscopic structures with different dimensions such as single-wall CNTs (SWCNTs), double-wall CNTs (DWCNTs), and multi-wall CNTs (MWCNTs). In this book chapter, a comprehensive discussion on the synthesis, characterization and further utilization of CNTs in metal oxide-based SC has been outlined. Here, the metal oxide can be 1D nanofibers, 2D thin films, and 3D aerogels. Further, a detailed study has been framed on the design methodology and fabrication techniques for the supercapacitor. Recently, various developments and state-of-the-art applications have been proposed for such structures wherein CNTs have been used as electrodes in flexible SCs with varied device configurations such as sandwiched and interdigital in-plane. Furthermore, the flexible CNT-based electrodes have shown great bendability, and compressibility, as well as a long cycle lifetime.

**Keywords:** CNTs, flexible supercapacitor, nanofibers, energy, electrodes, conductivity

## 1. Introduction

Recent advancement in the wearable technologies and portable electronics, for example, intelligent clothes, human-like electronic skins, flexible cell phones, and smart ornaments, and increasing interests of diverse scientific communities have developed a flexible supercapacitor (SCs) able to deliver high energy and power output [1–4]. However, the current commercial SC technology is too rigid and very difficult to fulfill the demands of flexible electronics. Thus, it is urgent and right time to develop flexible SCs, which can offer several advantages such as pliable, light-weighted, and mechanically robust [5–7]. It is well known that typical flexible SCs consist of different flexible electrodes developed in various device configurations [8–10]. The important key to construct the flexible SCs lies with the selection of electrodes with light weight and intrinsic flexibility. Generally, based on the charge storage mechanism, SCs are categorized into two different ways namely as electrical double layer capacitors and pseudocapacitors and both offer a high-power density and

a long cycling life [11–13]. The charge storage mechanism in pseudocapacitor is where conductive polymers and transition metal compounds are utilized as an active material and the faradic reactions proceed on the surface of electroactive species [14–16]. On the other hand, in the case of carbon-based nanomaterials, energy storage is due to the accumulation of electrostatic charge at electrode/electrolyte interface, and the performance of the device is strongly dependent on the effective surface area [17–19].

Several carbon-based materials are used in the SC as an electrode but one-dimensional (1D) carbon nanotubes (CNTs) have gained much more attention as it offers high-specific surface area that has great potential to fulfill the requirement for flexible SCs [20–22]. The  $sp^2$  hybridization in carbon-carbon (C-C) bonds supports the excellent mechanical strength of CNT, and better electronic and thermal conductivity along with chemical stability [23, 24]. The large aspect ratio (width-to-length ratio) and comparatively easy surface functionalization further make CNTs are more suitable candidate wherein different nanomaterials can be easily chemically attached [25, 26]. To date, several positive approaches have been implemented for the design and realization of CNT-based flexible SCs devices. CNTs exhibit excellent electrical conductivity, and ballistic ionic transport can be optimized by the mesostructured mesh-like frameworks when CNTs are stacked. These mesh-like frameworks offer a large surface area that minimizes charge redistribution and allows full-charge storage capacity at higher frequencies, as compared with porous carbons (PCs) or graphene [27–30]. Previously, different carbon composite films have been widely used to combine the complementary strengths such as CNTs and graphene composite has been demonstrated wherein good ionic conductivity and high volumetric energy density have been reported by utilizing the CNTs to PCs to enhance the electrical conductivity [31–33]. However, the electrical conductivity of the CNT mesostructured frameworks can be affected by the dispersion methods used in their synthesis [34–37].

In this book chapter, we provide a detailed comprehensive view of the current status and state-of-the-art achievements made in flexible SCs with CNT electrodes. Moreover, in this book chapter, various flexible CNT assemblies with different dimensions including 1D fibers, 2D films, and 3D aerogels have been discussed. Furthermore, we present a detailed summary of the CNT-based nanostructures that are utilized in flexible SCs device configurations. Finally, the current challenges and future outlook for the research opportunities on flexible SCs based on CNT electrodes are discussed.

## **2. Carbon nanotubes (CNTs)**

Herein, a detailed discussion about the classifications, useful properties such as electrical, mechanical, thermal, and electronics have been outlined in brief manner.

### **2.1 Classifications of CNTs**

As it is well known that the CNTs are the most powerful candidate from the carbon family, they play a very critical role to enhance the performance of various devices in various applications. For the classification point of view, CNTs can be classified into two types: (1) single-walled carbon nanotubes (SWCNTs) and (2) multi-walled carbon nanotubes (MWCNTs). In 1991, SWCNTs were accidentally synthesized by Iijima and Ichihashi [38] *via* arc-discharged method. The as-synthesized SWCNTs have a cylindrical structure made of one layer of graphene by folding it from

edge-to-edge. The effective diameter and length of the SWCNTs are nearly 1 nm and up to 1 mm, respectively. However, the production cost of the SWCNTs is more expensive, as compared to the MWCNTs [39]. On the other hand, a MWCNT has a concentric tube made of graphene sheets. The diameter of the MWCNT is varying in nature, as it is the multiple folds of the graphene sheets. As the MWCNT is made of the multiple folds to form concentric cylinders, the interplanar distance between each of the concentric cylinders is maintained by the internal Coulombic force and fixed in the range of 0.32 nm to 0.35 nm [40]. Here, it should be noted that the interplanar distance is nearly equal to the interplanar distance between two successive graphene layers in graphite [39]. However, for the electronic device applications, the utilization of MWCNTs is comparatively higher as compared to the SWCNTs as SWCNT has weaker adhesion profile with the used substrate surface [41]. On the other hand, in the case of MWCNTs, more active sites are available at the end of the tube [42] which further enhanced the adhesion properties of tube with the used substrate surface [41]. Sometimes, in the extreme case, MWCNT can also be considered as a double-walled carbon nanotube (DWCNT) wherein the formed structure is similar to the cylinders of the graphene layers with interlayer space of 0.335 nm. The physical and chemical properties of the DWCNT are very close to the SWCNT [39]. **Figure 1** depicts the illustration of SWCNTs, DWCNTs, and MWCNTs.

## 2.2 Properties of CNTs

In this section, the various remarkable properties of the CNTs such as electrical, mechanical, thermal, and electronics and its interrelation for utilizing areas of applications have been discussed.

### 2.2.1 Electrical properties of CNTs

The electrical properties of the CNTs are mainly utilized in electronics areas, as its show remarkable current density in order of  $10^9$  A/cm [44] and specific capacitance. The specific capacity of 25- $\mu\text{m}$ -thick CNT sheet electrode is found to be in the range of 39–90 F/cm<sup>3</sup> [45]. Moreover, CNTs can be behaved like a semiconductors or metal depending upon its structure [46]. The various electrical parameters of CNTs such as conductivity, resistivity [47], and capacitance [45] can be manipulated by functionalizing them with the appropriate chemical functional groups, as it creates defects over the CNTs surface. For example, the doping of gold nanoparticles in

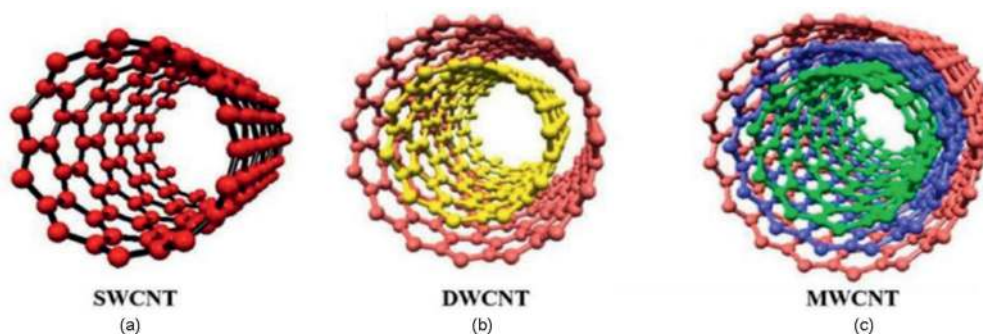


**Figure 1.** Illustration of (a) single-wall CNT, (b) double-wall CNT, (c) multi-wall CNT [43] © Applied Sciences 2021.

CNTs makes covalent bonds on its surface which further leads to the increment in conductivity [47].

To increase the electrochemical performance of the CNTs by opening the caps at the CNTs ends, chemical treatment can be performed [48]. On the other hand, under the heat treatment in the gaseous environment, the electrical conductivity of the CNTs is reduced due to the formation of  $sp^3$  bonds with the gaseous atoms [47]. It should be noted that the significant modulation in SWCNTs structure by enabling defects and functionalization shows 23% increment in the energy density, as compared to the graphite [42]. Moreover, variations in the electrical properties make change in the chirality factor, temperature, originating defects, and atmosphere change [47]. However, the electrical conduction in SWCNTs is comparatively lower than the MWCNTs [47]. The pure SWCNTs show electrical resistivity in the order of  $10^{-6} \Omega \cdot \text{cm}$ , while commercially available SWCNTs which are grown by chemical vapor deposition (CVD) showing an electrical resistivity in the range of  $1-7 \times 10^{-4} \Omega \cdot \text{cm}$  may be due to the presence of defects during manufacturing process.

Besides that, it is widely reported that the electrical properties of the CNTs are also varied due to their interfacial contact resistance [47], as it is created when two CNTs are connected in series. It is observed that if contact area between two CNTs increases, the contact resistance decreases. Due to its Schottky barrier connection with the matrix, it is a promising candidate for field emission transistors [49], as it enhances the recovery time and reduces the turn-on voltage.

### *2.2.2 Mechanical properties of CNTs*

The mechanical properties of CNTs are dependent on various production and structural factors such as the methods of production, the number of created defects, and structure, diameter, and symmetry of nanotubes [50, 51]. As reported [51], the arc discharge grown MWCNTs have higher mechanical strength, as compared to catalyst grown MWCNTs, which may be due to the fewer structural defects in arc-grown MWCNTs [51]. The covalent  $sp^2$  hybridization in CNT plays a major role in their strength [51] and due to this strong hybridization, MWCNTs can be bent at higher angles without destroying the structure [52]. Initially, it was very difficult to evaluate the mechanical strength of the CNTs due to its nanoscopic dimension but latterly, the transmission electron microscopy (TEM) is utilized to calculate the Young's modulus of SWCNTs and MWCNTs. Experimentally, for the MWCNTs, the observed highest Young's modulus is 4.15 TPa, and for the SWCNTs, it is around 1.3 TPa [51, 52]. However, the TEM method has many errors in measurement [30] and not provided accurate Young's modulus. Alternatively, atomic force microscopy (AFM) is used to obtain the Young's modulus in which pressure is applied on the CNTs *via* AFM tip made of  $\text{Si}_3\text{N}_4$  and corresponding load displacement curves have been plotted. As observed, MWCNTs with varying diameter in the range of 26–76 nm have shown a Young's modulus of  $1.28 \pm 0.5$  TPa and SWCNTs have nearly 1 TPa [51]. However, many researchers have used SWCNTs for the Young's modulus calculation because SWCNTs have fewer defects as compared to MWCNTs and, hence, exhibit more strength [52].

### *2.2.3 Thermal properties of CNTs*

The thermal properties of CNTs are dependent on the acoustic phonons of the nanotubes [53]. The mean free path of phonons helps to determine the range of



thermal conductivity of the CNTs [53]. As it is well known that the CNTs have a one-dimensional (1D) cylindrical tube structure by folding a two-dimensional (2D) graphene sheet, the phonon band structure becomes tough in the CNT [54]. The phonon density of states (P-DOS) is isolated in the isolated SWCNTs until the surrounding temperature must be low because the P-DOS is linearly depended on the specific heat above 1 K [53]. However, the temperature increases beyond 1 K, and the longitudinal and acoustic phonons increase, which further leads to the linear increment in specific heat. The value of specific heat in the SWCNT rope, 3D SWCNT, and graphene has found to be coincided and reflected phonon structure in 3D graphite at high temperature [54]. Moreover, certain experiments have been demonstrated in which thermal conductivity of CNTs were investigated at the room temperature and the obtained value is around 6600 W/mK [54]. On the other hand, the SWCNTs and MWCNTs have shown values of the thermal conductivities are 200 W/mK [54] and 3000 W/mK [53], respectively.

### **3. CNT-based metal oxide/sulfide thin film for flexible supercapacitor (SCs)**

Generally, flexible SCs architecture has two electrodes and polymer gel electrolyte is filled inside the electrode gaps. This gel electrolyte is playing the role of separator in the SCs configuration. Broadly, the SCs configuration can be categorized into three ways namely as (a) sandwiched architecture, (b) interdigital in-plane architecture, and (c) cable-type architecture. The different SCs configurations can be shown and utilized in different characteristics and applications. In the following sections, we have outlined the different device configurations facilitated with the CNT-based electrolytes.

#### **3.1 Sandwiched configuration**

The sandwiched configuration is the well-known and widely popular design in flexible SCs. However, previously flexible SCs faced problem with appropriate choice of electrolyte and electrodes, which can be avoid the usage of heavy current collectors. Kaempgen et al. [55] have reported the sprayed SWCNT thin films that act as both active electrodes and current collectors in bendable and ultralight SC device. The developed SC devices exhibited high values of specific capacitance, that is, 36 F/g due to the high electrical conductivity and porous channels under a discharge current density of 1 mA/cm<sup>2</sup>. Based on the internal resistance measurement analysis, there are no significant differences observed between the liquid H<sub>3</sub>PO<sub>4</sub> and solid PVA/H<sub>3</sub>PO<sub>4</sub> electrolyte. The obtained research outcomes confirm the feasibility of gel electrolyte as reported by previous studies [56, 57].

Further, Kanninen et al. [58] have developed a dry deposition technology to fabricate SWCNT thin films. Here, it should be noted that the fabricated bendable SCs exhibited a remarkable and favorable electrochemical property with high optical transparency up to 92%. The fabricated SCs devices may be used as a power source in smart transparent electronics such as display screen, sensor, and photovoltaic devices [59]. Therefore, the combination of CNTs with pseudocapacitive materials has proven efficient to improve the capacitance and energy density of flexible SCs and also maintain the robust mechanical behavior [20, 60, 61]. Here, **Figure 2** shows the sandwich structure-based SCs devices.

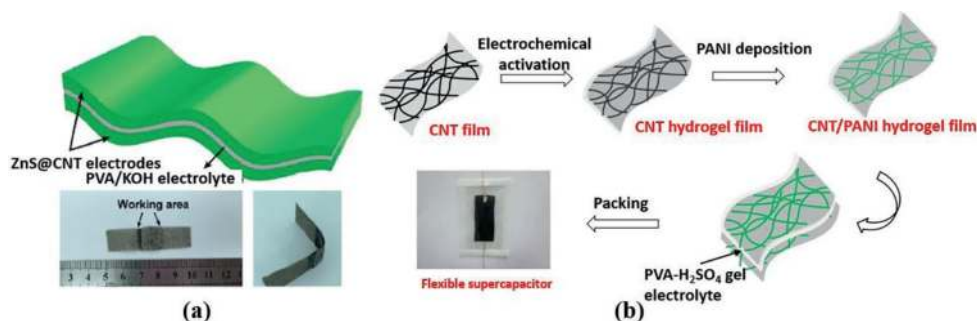


**Figure 2.**

(a) Schematic and photographs of the all-solid-state device with ZnS/CNT electrode [62], © Tsinghua University Press and Springer-Verlag Berlin Heidelberg 2017. (b) Fabrication process for flexible all-solid-state SC based on CNT/PANI hydrogel [63], © The Royal Society of Chemistry 2015.

### 3.2 Interdigital in-plane configuration

In the case of conventional sandwiched configuration, the electrodes usually suffer from large ion transport resistance, which may be induced from the thick and dense electrode design to store comparatively more energy. While in the case of interdigitated in-plane structural configuration, the electrode materials, current collectors, and gel electrolyte are on the same plane and the design methodology well addressing the issue related to the SCs for flexible electronics [64–67]. Moreover, interdigitated in-plane configuration offers fast ion transport *via* effectively controlling the interdigitated gap between the successive electrodes, which further helps to enhance the power density. Moreover, the ionic transport does not affect this configuration as it is in-plane structure and also supports the folding, rolling, and twisting [68, 69] without affecting the electrochemical performance of device. Therefore, in this section, we are focusing on the advanced SCs technologies that have been widely used for fabricating flexible SCs devices with interdigitated in-plane configuration by insertion of CNT to enhance the electrochemical performance.

Recently, Rani et al [70] have fabricated in-plane, interdigitated architecture-based microsupercapacitor (MSC) devices developed by utilizing electrophoretic deposition (EPD) wherein TiO<sub>2</sub> nanofibers (NFs) are used as an active electrode material and Mo is used as a current collector in interdigitated configuration for flexible electronic applications. In this reported work, TiO<sub>2</sub> NF is used as an active material, which offers one-dimensional (1D) nanostructured morphology and continuous nanofibric network, which can further provide the high electroactive surface area, reduced diffusion path length, and increased power density of the MSC device [71]. Further, to perform an EPD of active material, a disperse solution of TiO<sub>2</sub> NFs with 2 wt.% MWCNTs is prepared using ethanol [72] and deposited over Mo-coated PET substrate by applying a constant direct current (DC) voltage of 50 V. Moreover, TiO<sub>2</sub> is prominent candidates for the supercapacitor devices as it is economically viable and abundance in nature, and has structure-wise stability and environmentally friendly properties in various electronic applications [72]. Besides that, the utilized fabrication approach, that is, EPD offers several benefits for electrode fabrication such as cost-effectiveness, room temperature operation, better control over the process parameters, and no involvement of electrochemically inactive binder [72, 73]. The fabricated MSC device exhibited an excellent areal capacitance of ~9.4 mF/cm<sup>2</sup> [70].

Here, **Figure 3** shows the fabrication process flow, which is utilized during the fabricating of MSC device as reported by Rani et al [70].

Here, **Figure 4a** depicts the micrograph of surface of the active material-coated over the interdigitated electrode configuration of MSC device using the field emission scanning electron microscope (FESEM; Carl Zeiss). As seen in **Figure 4a**, it is clear that the  $\text{TiO}_2$  NFs and MWCNT are coated over the flexible Mo-coated PET substrate wherein MWCNTs form a highly dense conductive network between  $\text{TiO}_2$  NFs [72]. Further, due to entangled structure of MWCNTs, it helps to improve the electrical conductivity of the coated thin film of active material by creating electronic wiring between  $\text{TiO}_2$  NFs [72]. Furthermore, the cross-sectional analysis of fabricated structure is revealed that the device has compact electrode/electrolyte structure that further enhances the possibility of electrochemical stability of the fabricated device, as depicted in **Figure 4b**.

Further, Rani et al [70] have performed the electrochemical analysis for the fabricated MSCs device by utilizing cyclic voltammetry (CV) and galvanostatic charge/discharge (GCD) method by considering various scan rates and current densities, respectively, with potential window of 0–0.7 V. **Figure 5a** shows the CV curves for all the MSCs recorded at 10 mV/s scan rate which exhibit quasi-rectangular behavior. Herein, it should be noted that an enhanced area or also known as memory window of the CV curve for MSC3 device shows the improved capacitive performance as compared to MSC1 and MSC2 because in the case of MSC3 the reduction in ionic diffusion path by decreasing the interspace between adjacent interdigitated fingers further enables the faster diffusion of electrolytic ions inside the interspace [71, 75]. Besides that, the MSC4 device structure exhibited the highest electrochemical performance because it facilitated with minimum finger interspace (500  $\mu\text{m}$ ), which might reduce the ionic diffusion path and corresponding increment in the active sites as these significantly contributed to improve the electrochemical performance. Herein, **Figure 5b** depicts the galvanostatic charge/discharge curves for all the fabricated MSCs device

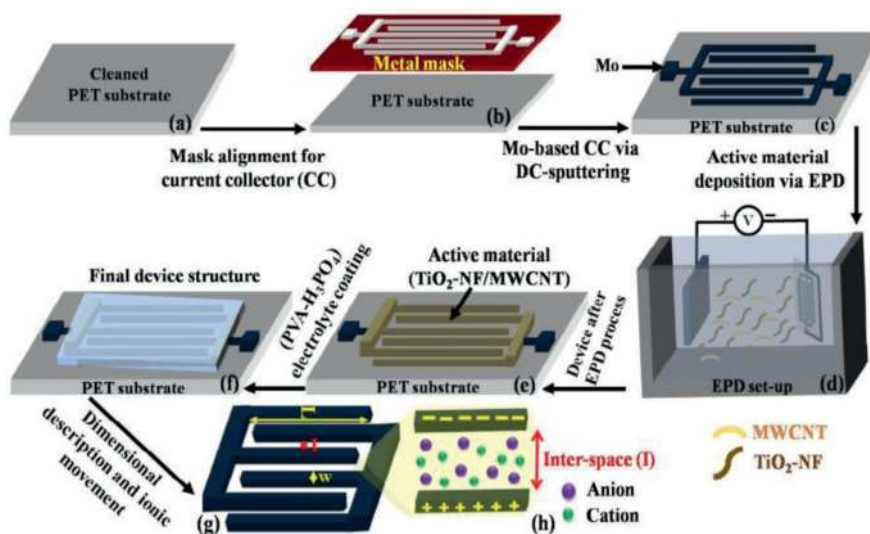


**Figure 3.** (a) Ultrasonically cleaned polyethylene terephthalate (PET) substrate. (b) Alignment of metal mask on cleaned PET substrate to pattern the current collector (CC). (c) Deposition of Mo metal contact on PET substrate. (d) Deposition of active materials on Mo-coated PET via EPD. (e) Active materials deposited MSC structure. (f) MSC device structure with gel electrolyte. (g) MSC structure with length and with description. (h) Illustration for ionic movement [70], © IEEE 2021.

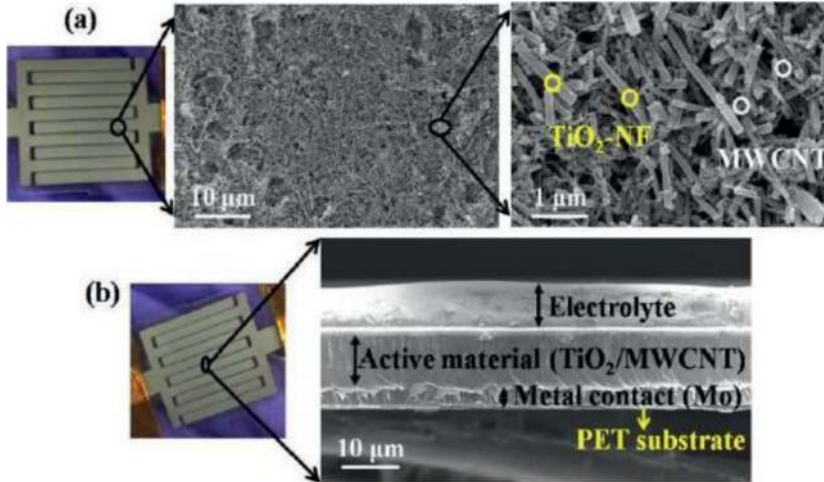


**Figure 4.** (a) Surface FESEM micrograph of MSC device. (b) Cross-sectional FESEM of MSC device [70], © IEEE 2021.

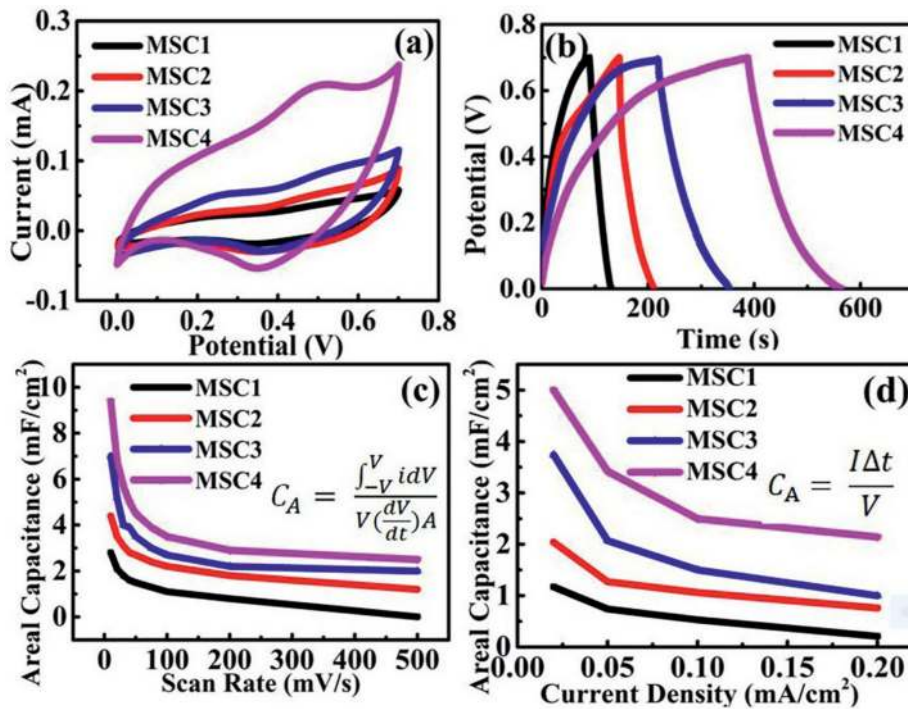


**Figure 5.** Electrochemical analysis of MSC devices. (a) Current-voltage curves at 10 mV/s scan rate. (b) GCD plots at 0.02 mA/cm<sup>2</sup> current density (*I*). (c)  $C_A$  vs. scan rates, and inset depicts the mathematical formulation used to calculate  $C_A$  (at mV/s), whereas  $dV/dt$  is the scan rate (V/s),  $i$ : current (mA),  $A$ : gel electrolyte coated active area (cm<sup>2</sup>) of MSC with fingers and their interspace, and  $V$ : voltage window (V) [74]. (d)  $C_A$  vs. current densities, and inset depicts the mathematical equation used to evaluate  $C_A$  (at mA/cm<sup>2</sup>), where  $I$ : current density (mA/cm<sup>2</sup>) and  $\Delta t$ : discharge time (s) [70, 72], © IEEE 2021.

structures that are not perfect in triangular shape as verified by the CV analysis [76]. It should be noted that the MSC4 device shows the maximum discharge time ( $\Delta t$ ) other than three MSC devices (MSC1, MSC2, and MSC3), which contributes in higher areal capacitance.



Here, **Figure 5c** shows the effect of scan rates on the areal capacitance of all MSCs structures. The areal capacitances vs. discharge current densities ( $I$ ) for all the MSCs are examined by their respective GCD curves as shown in **Figure 5d**. Here, it can be investigated that the MSC4 device structure shows better areal capacitances  $\sim 9.4 \text{ mF/cm}^2$  at  $10 \text{ mV/s}$  scan rate and  $\sim 5 \text{ mF/cm}^2$  at  $0.02 \text{ mA/cm}^2$  current density as depicted in **Figure 5c** and **d**. The enhanced values of the areal capacitance of the MSC device can also be correlated with the enhanced surface morphology of active material ( $\text{TiO}_2/\text{MWCNT}$ ) and optimized number of gaps considered at a particular EPD voltage [72]. Furthermore, the enhanced surface morphology helps to improve ionic transport in the active material, which further leads to the higher utilization of available active sites near to the interspace region and there is no requirement of the addition of inactive binder to enhance the electrochemical performance and, hence, further improves its charge storage properties [72]. The areal capacitance of MSC4 device is higher than many previously reported MSC devices [74, 77–81].

To examine the application of fabricated MSCs device in flexible electronics as an energy storage, various bending angles such as  $120^\circ$ ,  $135^\circ$ , and  $145^\circ$  have been investigated. As seen in **Figure 6a**, the CV curves for the MSC4 device at  $120^\circ$  and  $135^\circ$  bending angles show the minor changes in the CV area suggesting better flexibility of the device [71, 77]. Furthermore, under the bending conditions the long cyclability in MSC4 at  $0.2 \text{ mA/cm}^2$  for 2000 GCD cycles at  $145^\circ$  as shown in **Figure 6b** proves that the device is able to maintain nearly 73% capacitance retention, which further can be associated with the excellent flexibility of the device. However, the decrement in the capacitance retention under bending condition is associated with the increment in the resistance as shown in **Figure 6c** and corresponding decrement in the electrical conductivity of the active material film wherein the generation of cracks on the surface is caused by bending force [82].

Therefore, under the bending conditions it is more difficult for the electrolytic ions to move freely and come in contact with the available electroactive sites in active material. As a result, the areal capacitance of the MSC device is decreased as compared with the unbending state [83–85]. The fabricated interdigitated in-plane MSC device exhibited maximum areal energy density and areal power density are  $0.64 \text{ } \mu\text{Wh/cm}^2$  and  $307.2 \text{ } \mu\text{W/cm}^2$ , respectively, which are comparatively better than the previously published reports [74, 86–89] and the fabricated devices have potential applications in flexible microelectronic devices area with high performance and stability.

### 3.3 Cable-type configuration

Recently, cable-type configuration for SCs devices has gained very much attention from the scientific communities as these offer the excellent opportunity to enhance the mechanical property for portable/wearable electronics devices [90–92]. The straight cable's structure can be categorized into large-scale textiles for specific area applications [93, 94]. However, one of the major concerns for this SCs structure is to realize into linear-shaped electrode that can offer excellent flexibility along with desired capacitive properties. Therefore, by considering the striking physical and chemical properties, CNTs have been considered as a promising candidate in flexible SCs to enhance the electrochemical performance of the device.

Most recent, Rani et al [95] have developed all-solid-state flexible yarn SC (YSC) device by utilizing EPD technique wherein  $\text{TiO}_2$  NFs and MWCNTs are used as

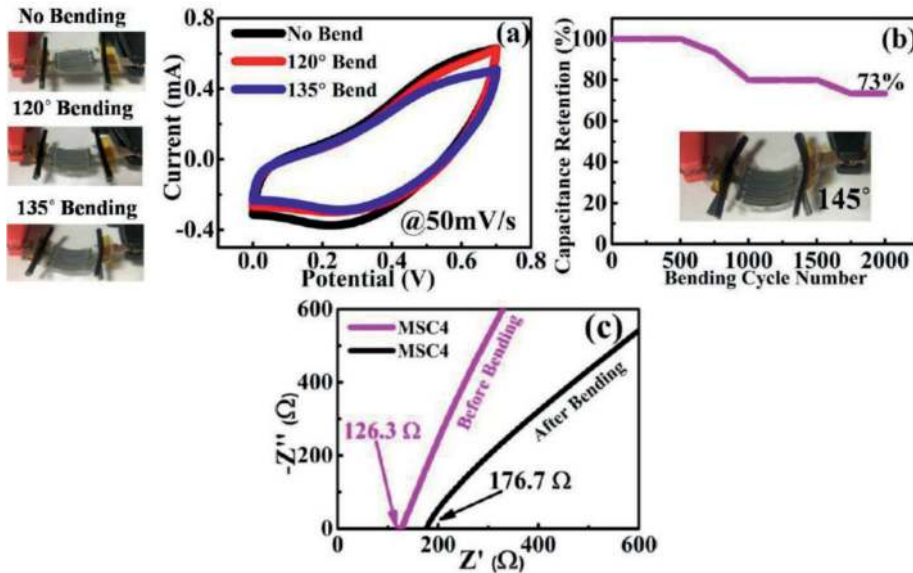


**Figure 6.** (a) Current-voltage plots for MSC4 device at various bending angles. (b) Capacitance retention curve of MSC4 at  $0.2 \text{ mA/cm}^2$  for 2000 GCD cycles at  $145^\circ$ . (c) Impedance spectroscopy analysis of MSC4 with and without bending cycles [70], © IEEE 2021.

an active material, while flexible and low-density carbon yarn is used as a current collector. Herein, to fabricate the YSC devices, the gel electrolyte is used. Further, to enhance the capacitance and the energy density of the YSC device, a small amount of redox additive is mixed into the gel electrolyte at room temperature. The as-fabricated YSC device exhibits the excellent electrochemical and mechanical flexibility. After the successful investigation of the electrochemical characteristics and mechanical flexibility of the fabricated device, three-similar YSCs are connected in series into a wearable fabric wherein a red LED is glowing for more than 5 min even under bending condition at different bending angles. Hence, the excellent electrochemical performance with and without bending further proves the potential applications in practical flexible and smart textile.

For the fabrication of the cable-type configuration SC, firstly,  $\text{TiO}_2$  NFs are synthesized by utilizing the facile electrospinning technique. The detailed synthesis process for the  $\text{TiO}_2$  NFs is outlined elsewhere [72]. After the synthesis of  $\text{TiO}_2$  NFs, a dispersed solution of  $\text{TiO}_2$  NFs is prepared into the ethanol through ultrasonication process and 2 wt.% MWCNTs are also mixed to improve the adhesion between  $\text{TiO}_2$  NFs to enhance the conductivity of the coated yarn electrode. Here, it should be noted that the surface of the active material must be electrically charged when it is dipped into dispersed solution as it moves toward the working electrode, which has opposite charge under the excitation of an external electric field in EPD process. Hence, a small quantity of charging additive; that is, hydrochloric acid  $\sim 100 \mu\text{L}$ , 36.4 wt.% is incorporated into the active material solution before ultrasonication to generate positive charges on the surface of the active material during cathodic EPD method.

The induced surface electric potential is measured *via* Malvern Zeta sizer Nano ZS90 system and known as a zeta potential which is 36 mV. Further, a commercial bare carbon is taken and cleaned *via* acetone and deionized (DI) water followed by heat treatment at  $450^\circ\text{C}$  temperature for 2 h to activate its surface for the deposition. The activated bare carbon yarn, as shown in **Figure 7a** is served as a cathode and

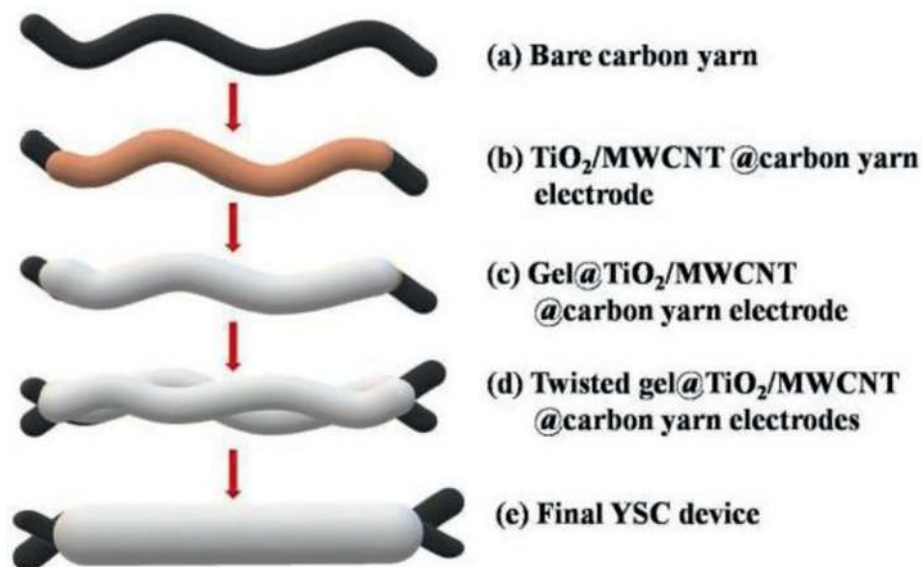


**Figure 7.** Step-by-step fabrication process for flexible YSC device [95], © IEEE 2022.

stainless steel is served as an anode. For the deposition, both electrodes are placed into the prepared disperse solution by keeping distance 1 cm between them and applied DC voltage of 50 V for 10-min supply. Furthermore, active material-coated yarn electrode is dried at 60°C temperature in vacuum for 12 h, as shown in **Figure 7b**.

The gel electrolyte has been prepared with polyvinyl alcohol (PVA: 6 g) powder and DI water (60 mL) and constantly stirred at 90°C to get a homogeneous and transparent solution and added 1 M H<sub>3</sub>PO<sub>4</sub> to the prepared solution with 40 mM sodium molybdate (Na<sub>2</sub>MoO<sub>4</sub>) mixed into the solution and stirred for 30 min. Next, for the fabrication of all-solid-state flexible YSC devices, two yarn electrodes with active material are dipped into the gel electrolyte for 1 h and dried at 30 °C for 12 h, as shown in **Figure 7c** and these two yarns are further twisted with each other to fabricate the YSC device, as depicted in **Figure 7d** and further coated with the gel electrolyte and dried at 30°C for 12 h, as shown in **Figure 7e**. Here, it should be noted that the gel acts as an electrolyte as well as the separator between two carbon yarn electrodes.

Here, **Figure 8** shows the surface morphology of the bare and coated carbon yarn electrodes that are investigated by FESEM analysis. **Figure 8a** and **b** clearly shows the difference between bare and coated carbon yarn wherein active material is densely

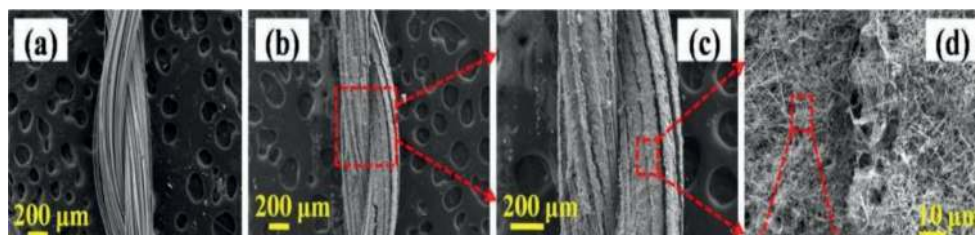


**Figure 8.** (a) FESEM image of bare carbon yarn electrode. (b-d) FESEM images of active material coated carbon yarn electrode, [95], © IEEE 2022.

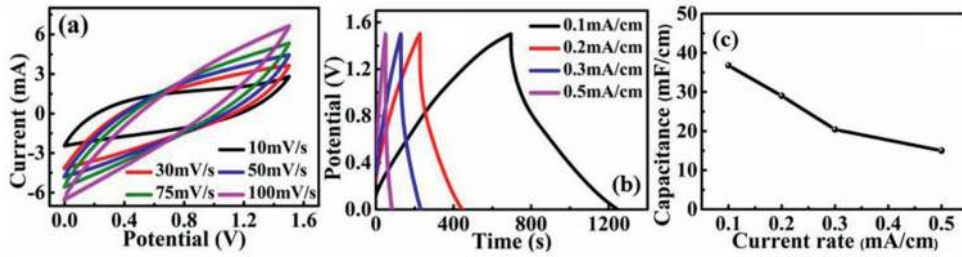


**Figure 9.** Electrochemical properties of YSC device: (a) CV plots at 10–100 mV/s sweep rates. (b) GCD data plots at 0.1–0.5 mA/cm current rates. (c) Rate capability graph, [95], © IEEE 2022.

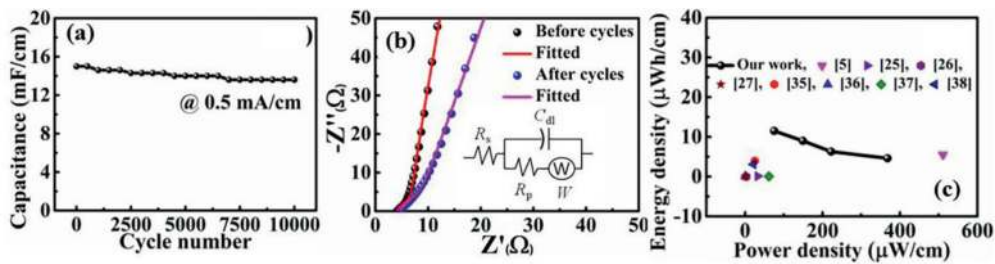


**Figure 10.** (a) Long cyclability graph, (b) EIS data plots (before and after cycling); inset displays the electrical equivalent circuit. (c) Energy density vs. power density of the YSC device in a Ragone plot [95], © IEEE 2022.

coated over the yarn surface, which acts as a current collector. **Figure 8c** and **d** depicts the enlarge FESEM image of the coated yarn.

After the morphological and structural analysis of the fabricated YSC device, the electrochemical analysis has been performed in two electrode configurations. The CV graphs for the fabricated YSC devices are exhibited in **Figure 9a** with varied sweep rate from 10 to 100 mV/s. The nature of obtained CV is similar to pseudocapacitive behavior and follows the same charge storage mechanism within the potential window of 0–1.5 V due to the involvement of the redox reactions and transfer of electrons on the surface as well as in the bulk of the active materials [72]. Further, the increment in the CV area is associated with the faster redox reaction at the higher sweep rate [96]. **Figure 9b** shows the GCD plots with different current rates ranging from 0.1 to 1.5 mA/cm, which are nearly triangular shapes and further confirm the pseudocapacitive charge storage mechanism, as outlined in **Figure 9a**.

The linear variations in YSC capacitances at different current rates are plotted in **Figure 9c** and as seen in **Figure 9c** and the maximum linear capacitance of the fabricated device is 36.8 mF/cm at 0.1 mA/cm current rate *via* GCD and 43.3 mF/cm at 10 mV/s *via* CV. At the higher current rates, the lower capacitance values are observed in **Figure 9c**, which may be due to the slower ionic diffusion of the electrolytic into the inner active site regions of the active material at higher applied current rates [72].

Next, to evaluate the cyclic stability of the fabricated YSC devices, a GCD analysis has been carried out at 0.5 mA/cm up to 10,000 cycles as shown in **Figure 10a**. Here, after the 10,000 cycles, the fabricated YSC devices exhibited 90% capacitance retention of its initial value which further confirmed the better stability for the device. Therefore, the higher linearity, areal, and volumetric capacitances and better cyclability of the YSC device have confirmed that the coated materials are highly dense and has hierarchical architecture of the active materials ( $\text{TiO}_2$  NFs and MWCNT) over



carbon yarns during the EPD process. Here, it should be noted that the hierarchical structure of the active materials is more favorable to improve the charge transport and ionic diffusion without binder materials as MWCNTs improve the electronic conduction by enabling the charge transportation in NFs network [70]. Therefore, the modified EPD-deposited architecture of the active materials ( $\text{TiO}_2$  NFs/MWCNT) can be added following features:

1. Modified EPD avoids the inactive binders;
2. Improves the movement of the electrolytic ions inside the active materials;
3. Improves the interface between electrode and electrolyte;
4. Improves the electrolytic ions transport by reducing diffusion path;
5. Minimizes the contact resistance between the substrate and the active materials;
6. Enables the active sites inside the active materials that improve the electrochemical performance.

Furthermore, to significantly increase the redox reaction, a little amount (5 mL) of  $\text{Na}_2\text{MoO}_4$  has been added into the PVA- $\text{H}_3\text{PO}_4$  gel electrolyte, which increases the capacitance and energy density of the fabricated YSC devices [97]. **Figure 10b** shows the cyclic stability of the fabricated YSC device before and after cycling wherein the impedance spectroscopy data are evaluated by utilizing ZView software and the examined data are displayed with their equivalent electrical circuit [98] in the inset of **Figure 10b**. In the equivalent electrical circuit,  $R_s$  signifies the ohmic resistance,  $R_p$  and  $C_{dl}$  denotes the faradic charge transfer resistance at the electrode/electrolyte interface and the double-layer capacitance, respectively, while  $W$  is associated with the Warburg impedance [99]. The two important terms such as energy and power densities are the very critical terms, which determine the performance of the SC devices. **Figure 10c** shows the energy and power densities of the fabricated devices as compared to the other reported literature [100–104].

Herein, **Figure 11** clearly depicts the role of active materials and MWCNTs in the performance of the YSC devices. As seen in **Figure 11a–c**, the electrochemical performance of the YSC devices is based on bare carbon yarns, MWCNT@carbon yarns, and  $\text{TiO}_2$  NFs@carbon yarns, wherein bare carbon yarns, MWCNT@carbon

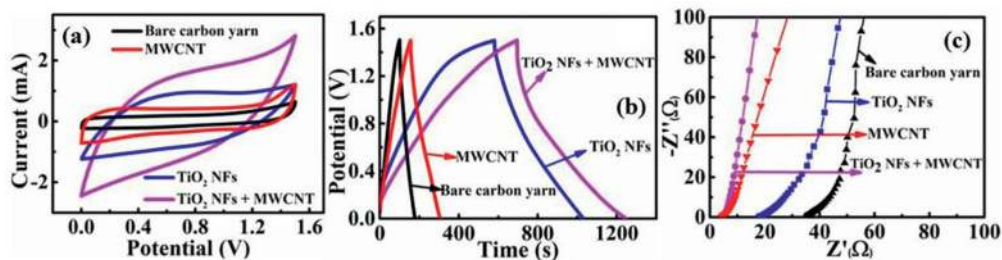


**Figure 11.** Performance of bare and active materials coated yarn device: (a) CV curves at 10 mV/s. (b) GCD curves at 0.1 mA/cm. (c) EIS data plots, [95], © IEEE 2022.

yarns, and TiO<sub>2</sub> NFs@carbon yarns depict the capacitance values of 5, 10, and 31 mF/cm, respectively, at 0.1 mA/cm.

To realize the particle applications, the fabricated YSC device structure must exhibit the better flexibility and mechanical bending stability against the varied bending angle to use as a power source in textile-based wearable/portable electronics applications. Therefore, to analysis the capability of the flexible YSC device structure to store and release the energy in the flexible electronics system, the electrochemical characterizations have been carried out under different bending states. **Figure 12a** shows the YSC device under different angles of bending, such as 0°, 45°, 90°, and 145°. It can be observed that the under the different bending angles the CV response of the fabricate devices has not been affected effectively, as shown in **Figure 12b**, and, hence, retains its supercapacitive behavior [71]. Further, the capacitive retention has also been analyzed under bending condition of 145° for 2000 cycles at 0.5 mA/cm *via* GCD as shown in **Figure 12c** and after 2,000 cycles, YSC device attends 95% of its initial capacitance, showing remarkable mechanical stability. Moreover, the robustness and durability of the YSC device is also associated with the superior flexibility and mechanical strength of the carbon yarn as a current collector, and the gel electrolyte which tightly bound all the components of the device to improve its electrochemical performance under extreme bending conditions. Herein, **Figure 12d–e** shows the CV and GCD plots for three similar YSC devices are fixed in a wearable fabric under series connection. As observed, the CV and GCD curves of series-connected YSCs at 10 mV/s and 0.1 mA/cm, respectively. The series-connected YSCs has successfully

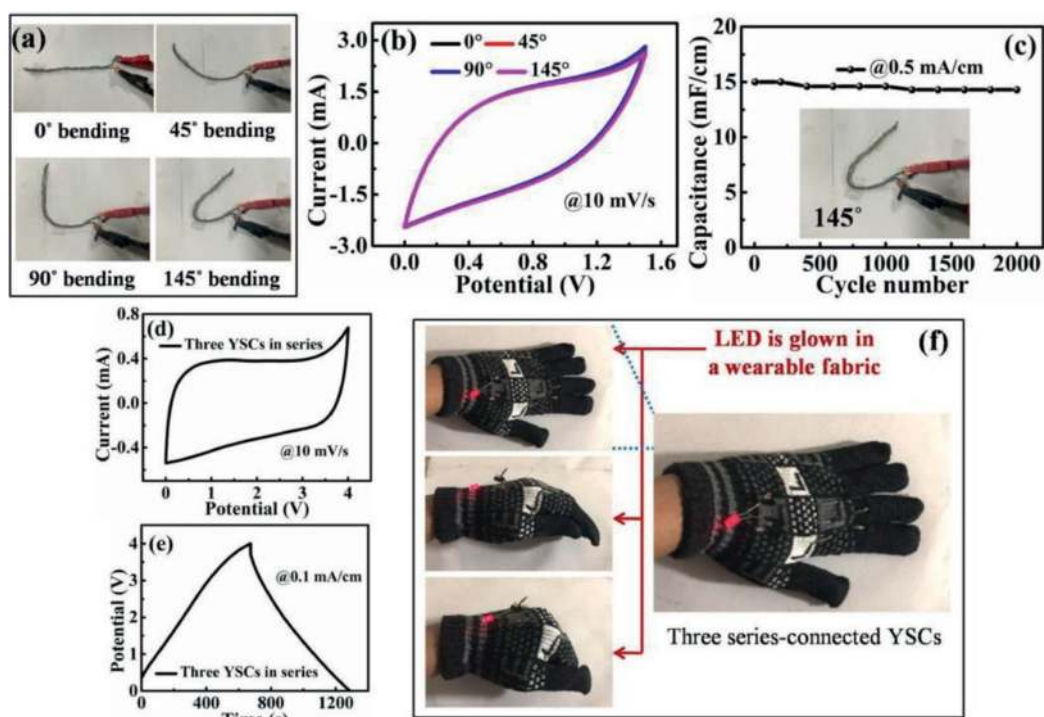


**Figure 12.**

(a) Various bending angles of the flexible YSC device, (b) current-voltage plots (@10 mV/s) for YSC device at different bending stages, (c) cyclability plot of YSC up to 2000 GCD cycles at 0.5 mA/cm at 145° bending angle. (d) CV curve (@10 mV/s) of three series-connected YSCs devices. (e) GCD curve (@0.1 mA/cm) of three series-connected YSCs devices. (f) Three series-connected YSCs devices fixed into a wearable fabric and glow a red LED at different bending states, [95], © IEEE 2022.

lighted a red LED under bending conditions at different bending angles for more than 5 min, as depicted in **Figure 12f**. Therefore, after the analyzing of characterized data, it can be concluded that the fabricated devices are much compatible with the wearable, flexible, and portable electronic devices.

#### 4. Conclusions and future perspectives

In summary, the rapid development of portable and wearable electronics has opened the new opportunities for miniaturized flexible SCs. The unique cylindrical shape and remarkable and excellent mechanical properties are toward stability and bendability of the CNTs to form flexible interconnected network within the active materials. Several synthesis and fabrication processes such as electrospinning, EPD, and hydrothermal and solution process have been utilized to synthesize the active materials and CNTs to develop the flexible SCs device to fulfill the demand of the current flexible electronic market. In the pseudocapacitive materials, CNTs can also be incorporated to improve the electrochemical performance of the fabricated flexible devices. Moreover, different device configurations such as sandwiched, interdigital in-plane, and cable-type have been widely investigated as per the desired applications. The involvement of flexible CNTs into electrode and active materials helps to enhance the high flexibility in SCs that are bendable or foldable, stretchable or compressible, wearable, and twistable and under all the extreme conditions, the fabricated devices are to maintain the electrochemical performance of the energy storage devices. Based the configurations, the sandwiched SCs are extensively studied as it has simple device structure but poor electrochemical performance due to the lower rate of ionic transport. While in the case of interdigital in-plane device structure, wherein fast ionic transport can be facilitated *via* optimized and well-controlled gap distances between interdigitated electrode fingers without hindering the ion transport. The cable-type configuration also facilitated to maximize the mechanical property, which further enables the flexibility and bendability of the fabricated devices.

Specifically, the incorporation of CNTs nanostructured into metal oxide nanofibers/nanobelts/nanotubes attended the higher areal and specific capacitance that are the backbone of the any energy storage devices especially in the case of flexible SCs. However, accelerated progresses have been achieved in flexible SCs devices, which are equipped with CNT materials but some critical challenges are still exist, which are extensively need to be addressed to realize these for their practical applications. The solid-state electrolyte is the key component of flexible SCs, and currently available solid state gel electrolytes have issues with high viscosity and low ionic conductivity that further limited the power output of flexible SCs. Therefore, a novel solid-state electrolyte who can support high ionic conductivity and excellent mechanical behavior is required to accelerate the flexible SC research. However, the electrochemical mechanism in CNTs-oriented solid-state electrolyte for flexible devices is still unclear and it is essentially required to understand the correct energy storage mechanism to design and fabricate of more effective flexible SCs. It should be noted that the large-scale preparation of CNTs nanotube and fibers by utilizing wet/dry spinning techniques are readily available, which can hold the great potential to facilitate the application of flexible SCs. We strongly believe that research and development in these areas will be beneficial and significantly contribute to the development and commercialization of flexible SCs in the near future.

## **Conflict of interest**

The authors declare no conflict of interest.

## **Author details**

Shalu Rani<sup>1\*</sup>, Sanjay Kumar<sup>2</sup> and Ritesh Bhardwaj<sup>3</sup>

1 Centre of Nanotechnology, Indian Institute of Technology Roorkee, Roorkee, India


2 Department of Electrical Engineering, Indian Institute of Technology Indore, Indore, Madhya Pradesh, India

3 Department of Electronics and Communication Engineering, Dr. B. R. Ambedkar National Institute of Technology, Jalandhar, Punjab, India

\*Address all correspondence to: shalu29singh@gmail.com

## **IntechOpen**

---

© 2022 The Author(s). Licensee IntechOpen. This chapter is distributed under the terms of the Creative Commons Attribution License (<http://creativecommons.org/licenses/by/3.0>), which permits unrestricted use, distribution, and reproduction in any medium, provided the original work is properly cited. 



## References

- [1] Shao YL, El-Kady MF, Wang LJ, Zhang QH, Li YG, Wang HZ, et al. Graphene-based materials for flexible supercapacitors. *Chemical Society Reviews*. 2015;44:3639-3665
- [2] Ko Y, Kwon M, Bae WK, Lee B, Lee SW, Cho J. Flexible supercapacitor electrodes based on real metal-like cellulose papers. *Nature Communications*. 2017;8:536
- [3] Wang YQ, Ding Y, Guo XL, Yu GH. Conductive polymers for stretchable supercapacitors. *Nano Research*. 2019;12:1978-1987
- [4] Li WW, Gao FX, Wang XQ, Zhang N, Ma MM. Strong and robust polyaniline-based supramolecular hydrogels for flexible supercapacitors. *Angewandte Chemie International Edition*. 2016;55:9196-9201
- [5] Liu LL, Niu ZQ, Chen J. Design and integration of flexible planar micro-supercapacitors. *Nano Research*. 2017;10:1524-1544
- [6] Liu LL, Niu ZQ, Chen J. Flexible supercapacitors based on carbon nanotubes. *Chinese Chemical Letters*. 2018;29:571-581
- [7] Huang P, Lethien C, Pinaud S, Brousse K, Laloo R, Turq V, et al. On-chip and freestanding elastic carbon films for micro-supercapacitors. *Science*. 2016;351:691-695
- [8] El-Kady MF, Strong V, Dubin S, Kaner RB. Laser scribing of high-performance and flexible graphene-based electrochemical capacitors. *Science*. 2012;335:1326-1330
- [9] Zhu S, Li YT, Zhu HY, Ni JF, Li Y. Pencil-drawing skinmountable micro-supercapacitors. *Small*. 2019;15:1804037
- [10] Fu YP, Cai X, Wu HW, Lv ZB, Hou SC, Peng M, et al. Fiber supercapacitors utilizing pen ink for flexible/wearable energy storage. *Advanced Materials*. 2012;24:5713-5718
- [11] Salanne M, Rotenberg B, Naoi K, Kaneko K, Taberna PL, Grey CP, et al. Efficient storage mechanisms for building better supercapacitors. *Nature Energy*. 2016;1:16070
- [12] Zhu S, Wang ZD, Huang FZ, Zhang H, Li SK. Hierarchical Cu(OH)<sub>2</sub>@Ni<sub>2</sub>(OH)<sub>2</sub>CO<sub>3</sub> core/shell nanowire arrays in situ grown on three-dimensional copper foam for high-performance solid-state supercapacitors. *Journal of Materials Chemistry A*. 2017;5:9960-9969
- [13] El-Kady MF, Shao YL, Kaner RB. Graphene for batteries, supercapacitors and beyond. *Nature Reviews Materials*. 2016;1:16033
- [14] Dubal DP, Ayyad O, Ruiz V, Gomez-Romero P. Hybrid energy storage: The merging of battery and supercapacitor chemistries. *Chemical Society Reviews*. 2015;44:1777-1790
- [15] Wu CZ, Lu XL, Peng LL, Xu K, Peng X, Huang JL, et al. Two-dimensional vanadyl phosphate ultrathin nanosheets for high energy density and flexible pseudocapacitors. *Nature Communications*. 2013;4:2431
- [16] Zuo WH, Li RZ, Zhou C, Li YY, Xia JL, Liu JP. Battery-supercapacitor hybrid devices: Recent progress and future prospects. *Advancement of Science*. 2017;4:1600539

- [17] Borenstein A, Hanna O, Attias R, Luski S, Brousse T, Aurbach D. Carbon-based composite materials for supercapacitor electrodes: A review. *Journal of Materials Chemistry A*. 2017;**5**:12653-12672
- [18] Ni JF, Li Y. Carbon nanomaterials in different dimensions for electrochemical energy storage. *Advanced Energy Materials*. 2016;**6**:1600278
- [19] Zhu S, Wu M, Ge MH, Zhang H, Li SK, Li CH. Design and construction of three-dimensional CuO/polyaniline/rGO ternary hierarchical architectures for high performance supercapacitors. *Journal of Power Sources*. 2016;**306**:593-601
- [20] Sun GZ, Zhang X, Lin RZ, Yang J, Zhang H, Chen P. Hybrid fibers made of molybdenum disulfide, reduced graphene oxide, and multi-walled carbon nanotubes for solid-state, flexible, asymmetric supercapacitors. *Angewandte Chemie, International Edition*. 2015;**54**:4651-4656
- [21] Zhou QY, Fan TW, Li YY, Chen DC, Liu SL, Li X. Hollow-structure NiCo hydroxide/carbon nanotube composite for high-performance supercapacitors. *Journal of Power Sources*. 2019;**426**:111-115
- [22] Zhou YS, Zhu YC, Xu BS, Zhang XJ. High electroactive material loading on a carbon nanotube/carbon nanofiber as an advanced free-standing electrode for asymmetric supercapacitors. *Chemical Communications*. 2019;**55**:4083-4086
- [23] Dalton AB, Collins S, Munoz E, Razal JM, Ebron VH, Ferraris JP, et al. Supertough carbon-nanotube fibres. *Nature*. 2003;**423**:703
- [24] Zeng YX, Zhang XY, Qin RF, Liu XQ, Fang PP, Zheng DZ, et al. Dendrite-free zinc deposition induced by multifunctional CNT frameworks for stable flexible Zn-ion batteries. *Advanced Materials*. 2019;**31**:1903675
- [25] Ni JF, Wang GB, Yang J, Gao DL, Chen JT, Gao LJ, et al. Carbon nanotube-wired and oxygen-deficient MoO<sub>3</sub> nanobelts with enhanced lithium-storage capability. *Journal of Power Sources*. 2014;**247**:90-94
- [26] Jin Q, Jiang S, Zhao Y, Wang D, Qiu JH, Tang DM, et al. Flexible layer-structured Bi<sub>2</sub>Te<sub>3</sub> thermoelectric on a carbon nanotube scaffold. *Nature Materials*. 2019;**18**:62-68
- [27] Black J, Andreas HA. Effects of charge redistribution on self-discharge of electrochemical capacitors. *Electrochimica Acta*. 2009;**54**:3568-3574
- [28] Taberna PL, Portet C, Simon P. Electrode surface treatment and electrochemical impedance spectroscopy study on carbon/carbon supercapacitors. *Applied Physics A: Materials Science & Processing*. 2006;**82**:639-646
- [29] Frackowiak E. Carbon materials for supercapacitor application. *Physical Chemistry Chemical Physics*. 2007;**9**:1774-1785
- [30] Dinh TM, Armstrong K, Guay D, Pech D. High-resolution on-chip supercapacitors with ultra-high scan rate ability. *Journal of Materials Chemistry A*. 2014;**2**:7170-7174
- [31] Zhu Y, Murali S, Stoller MD, Ganesh KJ, Cai W, Ferreira PJ, et al. Carbon-based supercapacitors produced by activation of graphene. *Science*. 2011;**332**:1537-1541
- [32] Kim TY, Jung G, Yoo S, Suh KS, Ruoff RS. Activated graphene-based carbons as supercapacitor electrodes

- with macro- and mesopores. *ACS Nano*. 2013;**7**:6899-6905
- [33] Zhang LL, Zhao X, Stoller MD, Zhu Y, Ji H, Murali S, et al. Highly conductive and porous activated reduced graphene oxide films for high-power supercapacitors. *Nano Letters*. 2012;**12**:1806-1812
- [34] Niu C, Sichel EK, Hoch R, Moy D, Tennent H. High power electrochemical capacitors based on carbon nanotube electrodes. *Applied Physics Letters*. 1997;**70**:1480-1482
- [35] Simon P, Gogotsi Y. Charge storage mechanism in nanoporous carbons and its consequence for electrical double layer capacitors. *Philosophical Transaction on Royal Society A*. 2010B;**368**:3457-3467
- [36] Tung VC, Chen LM, Allen MJ, Wassei JK, Nelson K, Kaner RB, et al. Low-temperature solution processing of graphene-carbon nanotube hybrid materials for high-performance transparent conductors. *Nano Letters*. 2009;**9**:1949-1955
- [37] Xu Z, Li Z, Holt CMB, Tan X, Wang H, Amirkhiz BS, et al. Electrochemical supercapacitor electrodes from sponge-like graphene nanoarchitectures with ultrahigh power density. *Journal of Physical Chemistry Letters*. 2012;**3**:2928-2933
- [38] Iijima S, Ichihashi T. Single-shell carbon nanotubes of 1-Nm diameter. *Nature*. 1993;**363**:603
- [39] Saifuddin N, Raziah AZ, Junizah AR. Carbon nanotubes: A review on structure and their interaction with proteins. *Journal of Chemistry*. 2013;**67**:6815
- [40] Kharissova OV, Kharisov BI. Variations of interlayer spacing in carbon nanotubes. *RSC Advances*. 2014;**4**:30807
- [41] Bichoutskaia E, Popov AM, Lozovik YE. Nanotube-based data. *Insight*. 2008;**11**:38
- [42] Kohler AR, Som C, Helland A, Gottschalk F. Studying the potential release of carbon nanotubes throughout the application life cycle. *Journal of Cleaner Production*. 2008;**16**:927
- [43] Rathinavel S, Priyadharshini K, Panda D. A review on carbon nanotube: An overview of synthesis, properties, functionalization, characterization, and the application. *Materials Science and Engineering B*. 2021;**268**:115095
- [44] Tanabi H, Erdal M. Effect of CNTs dispersion on electrical, mechanical and strain sensing properties of CNT/Epoxy nanocomposites. *Results Physics*. 2019;**12**:486
- [45] Ma R, Wei B, Xu C, Liang J, Wu D. Development of supercapacitors based on carbon nanotubes. *Science in China, Series E Technological Sciences*. 2020;**43**:178
- [46] Zeng Q, Li Z, Zhou Y. Synthesis and application of carbon nanotubes. *Journal of Natural Gas Chemistry*. 2006;**15**:235
- [47] Li Q, Li Y, Zhang X, Chikkannanavar SB, Zhao Y, Dangelewicz AM, et al. Structure-dependent electrical properties of carbon nanotube fibers. *Advanced Materials*. 2007;**19**:3358
- [48] Fu YB, Ma RB, Chen YM, Jiang DD, Zhang QY, Ma XH. The effect of acidic treatment on the lithium storage capacity of multi-walled carbon nanotubes. *Journal of Materials Science: Materials in Electronics*. 2007;**20**:709
- [49] Robertson J. Growth of nanotubes the roadmap for semiconductor devices

- envisages that carbon. Review: Literature and Arts of the Americas. 2007;**10**:36
- [50] Grobert N. Carbon nanotubes – importance of clean CNT material for the success of future applications. *Materials Today*. 2007;**10**:28
- [51] Salvetat JP, Bonard JM, Thomson NH, Kulik AJ, Forro L, Benoit W, et al. Mechanical properties of carbon nanotubes. *Applied Physics A: Materials Science & Processing*. 1999;**69**:255
- [52] Someya T, Small J, Kim P, Nuckolls C, Yardley JT. Alcohol vapor sensors based on single-walled carbon nanotube field effect transistors. *Nano Letters*. 2003;**3**:877
- [53] Popov VN. Carbon nanotubes: Properties and application. *Materials Science Engineering Report*. 2004;**43**:61
- [54] Hone J, Llaguno MC, Biercuk MJ, Johnson AT, Batlogg B, Benes Z, et al. Thermal properties of carbon nanotubes and nanotube-based materials. *Applied Physics A: Materials Science & Processing*. 2002;**74**:339
- [55] Kaempgen M, Chan CK, Ma J, Cui Y, Gruner G. Printable thin film supercapacitors using single-walled carbon nanotubes. *Nano Letters*. 2009;**9**:1872-1876
- [56] Vincent C. Polymer electrolytes. *Progress in Solid State Chemistry*. 1987;**17**:145-261
- [57] Nohara S, Wada H, Furukawa N, Inoue H, Morita M, Iwakura C. Electrochemical characterization of new electric double layer capacitor with polymer hydrogel electrolyte. *Electrochimica Acta*. 2003;**48**:749-753
- [58] Kanninen P, Luong ND, Sinh LH, Anoshkin IV, Tsapenko A, Seppala J, et al. Transparent and flexible high-performance supercapacitors based on single-walled carbon nanotube films. *Nanotechnology*. 2016;**27**:235403
- [59] Zhu S, Ni J, Li Y. Carbon nanotube-based electrodes for flexible supercapacitors. *Nano Research*. 2020;**13**:7
- [60] Jiang YC, Wu ZY, Jiang L, Pan ZC, Yang PY, Tian WC, et al. Freestanding CoSeO<sub>3</sub>·H<sub>2</sub>O nanoribbon/carbon nanotube composite paper for 2.4 V high-voltage, flexible, solid-state supercapacitors. *Nanoscale*. 2018;**10**:12003-12010
- [61] Wang Q, Wang HX, Du PC, Liu JL, Liu D, Liu P. Porous polylactic acid/carbon nanotubes/polyaniline composite film as flexible free-standing electrode for supercapacitors. *Electrochimica Acta*. 2019;**294**:312-324
- [62] Hou XY, Peng T, Cheng JB, Yu QH, Luo RJ, Lu Y, et al. Ultrathin ZnS nanosheet/carbon nanotube hybrid electrode for high-performance flexible all-solid-state supercapacitor. *Nano Research*. 2017;**10**:2570-2583
- [63] Zeng S, Chen HY, Cai F, Kang YR, Chen MH, Li QW. Electrochemical fabrication of carbon nanotube/polyaniline hydrogel film for all-solid-state flexible supercapacitor with high areal capacitance. *Journal of Materials Chemistry A*. 2015;**3**:23864-23870
- [64] Guo RS, Chen JT, Yang BJ, Liu LY, Su LJ, Shen BS, et al. In-plane micro-supercapacitors for an integrated device on one piece of paper. *Advanced Functional Materials*. 2017;**27**:1702394
- [65] Liu ZY, Wu ZS, Yang S, Dong RH, Feng XL, Mullen K. Ultraflexible in-plane micro-supercapacitors by direct printing of solution-processable



- electrochemically exfoliated graphene. *Advanced Materials*. 2016;**28**:2217-2222
- [66] Du JW, Mu XM, Zhao YR, Zhang YX, Zhang SM, Huang BY, et al. Layered coating of ultraflexible graphene-based electrodes for high-performance in-plane quasi-solid-state micro-supercapacitors. *Nanoscale*. 2019;**11**:14392-14399
- [67] Liu NS, Gao YH. Recent progress in micro-supercapacitors with in-plane interdigital electrode architecture. *Small*. 2017;**13**:1701989
- [68] Pu X, Liu MM, Li LX, Han SC, Li XL, Jiang CY, et al. Wearable textile-based in-plane microsupercapacitors. *Advanced Energy Materials*. 2016;**6**:1601254
- [69] Li JH, Shi QW, Shao YL, Hou CY, Li YG, Zhang QH, et al. Cladding nanostructured AgNWs-MoS<sub>2</sub> electrode material for high-rate and long-life transparent in-plane micro-supercapacitor. *Energy Storage Mater*. 2019;**16**:212-219
- [70] Rani S, Kumar N, Tandon A, Sharma Y. Electrophoretic grown TiO<sub>2</sub>-based interdigitated microsupercapacitor: Device fabrication and characterization for flexible electronics. *IEEE Transactions on Electron Devices*. 2021;**68**:10
- [71] Song Y, Chen XX, Zhang JX, Cheng XL, Zhang HX. Freestanding micro-supercapacitor with interdigital electrodes for low power electronic systems. *Journal of Microelectromechanical System*. 2017;**26**:1055
- [72] Rani S, Kumar N, Tandon A, Sharma Y. Fabrication of binder free TiO<sub>2</sub> nanofiber electrodes via electrophoretic deposition for low power electronic applications. *IEEE Transactions on Electron Devices*. 2021;**68**:251
- [73] Chen CC et al. Performance enhancement on an InGaP/InGaAs PHEMT with an electrophoretic deposition gate structure. *IEEE Electronic Device Letters*. 2014;**35**:18
- [74] Singh BK, Shaikh A, Dusane RO, Parida S. Nanoporous Gold-Nitrogen-doped carbon nano-onions all-solid-state microsupercapacitor. *Nano-Struct. Nano-Objects*. 2019;**17**:239-247
- [75] Rani S, Kumar N, Sharma Y. Recent progress and future perspectives for the development of micro-supercapacitors for portable/wearable electronics applications. *Journal of Physics Energy*. 2021;**3**:230
- [76] Kumar N, Singh M, Kumar A, Tseng TY, Sharma Y. Facile and one-step in situ synthesis of pure phase mesoporous Li<sub>2</sub>MnSiO<sub>4</sub>/CNTs nanocomposite for hybrid supercapacitors. *ACS Applied Energy Materials*. 2020;**3**:2450-2464
- [77] Boruah BD, Maji A, Misra A. Flexible array of microsupercapacitor for additive energy storage performance over a large area. *ACS Applied Materials & Interfaces*. 2018;**10**:15864-15872
- [78] Zhang L et al. Photolithographic fabrication of graphene-based all-solid-state planar on-chip microsupercapacitors with ultrahigh power characteristics. *Journal of Applied Physics*. 2019;**126**:16
- [79] Lee KH, Lee SS, Ahn DB, Lee J, Byun D, Lee SY. Ultrahigh areal number density solid-state on-chip microsupercapacitors via electrohydrodynamic jet printing. *Science Advances*. 2020;**6**:eaaz16
- [80] Wang J, Wang X, Lee SW, Zhang Q. Enhanced performance of an electric double layer microsupercapacitor

based on novel carbon encapsulated cu nanowire network structure as the electrode. *ACS Applied Materials Interface*. 2019;**11**:43

[81] Chen T, Dai L. Flexible and wearable wire-shaped micro-supercapacitors based on highly aligned Titania and carbon nanotubes. *Energy Storage Mater*. 2016;**2**:21-26

[82] Jeong HT, Du JF, Kim YR. Development of flexible energy storage device by using polymer electrolyte based on ionic liquid. *ChemistrySelect*. 2017;**2**:6057-6061

[83] Zhang J, Dong L, Xu C, Hao J, Kang F, Li J. Comprehensive approaches to three-dimensional flexible supercapacitor electrodes based on MnO<sub>2</sub>/carbon nanotube/activated carbon fiber felt. *Journal of Material Science*. 2017;**52**:5788-5798

[84] Iqbal N, Wang X, Babar AA, Zainab G, Yu J, Ding B. Flexible Fe<sub>3</sub>O<sub>4</sub> carbon nanofibers hierarchically assembled with MnO<sub>2</sub> particles for high-performance supercapacitor electrodes. *Scientific Reports*. 2017;**7**:15153

[85] Li X et al. High energy flexible supercapacitors formed via bottom-up infilling of gel electrolytes into thick porous electrodes. *Nature Communications*. 2018;**9**:1

[86] Lee K, Lee H, Shin Y, Yoon Y, Kim D, Lee H. Highly transparent and flexible supercapacitors using graphene-graphene quantum dots chelate. *Nano Energy*. 2016;**26**:746-754

[87] Lee G et al. Fully biodegradable micro-supercapacitor for power storage in transient electronics. *Advanced Energy Materials*. 2017;**7**:1700157

[88] Liu W et al. Paper-based all-solid-state flexible micro-supercapacitors

with ultra-high rate and rapid frequency response capabilities. *Journal of Material Chemistry A*. 2016;**10**:3754

[89] Zhang CJ et al. Stamping of flexible, coplanar micro-supercapacitors using MXene inks. *Advanced Functional Materials*. 2018;**28**:1705506

[90] Lee SY, Choi KH, Choi WS, Kwon YH, Jung HR, Shin HC, et al. Progress in flexible energy storage and conversion systems, with a focus on cable-type lithium-ion batteries. *Energy & Environmental Science*. 2013;**6**:2414-2423

[91] Vellacheri R, Zhao HP, Muhlstadt M, Al-Haddad A, Jandt KD, Lei Y. Rationally engineered electrodes for a high-performance solid-state cable-type supercapacitor. *Advanced Functional Materials*. 2017;**27**:1606696

[92] Chen YJ, Xu BG, Wen JF, Gong JL, Hua T, Kan CW, et al. Design of novel wearable, stretchable, and waterproof cable-type supercapacitors based on high-performance nickel cobalt sulfide-coated etching-annealed yarn electrodes. *Small*. 2018;**14**:1704373

[93] Pu X, Li LX, Liu MM, Jiang CY, Du CH, Zhao ZF, et al. Wearable self-charging power textile based on flexible yarn supercapacitors and fabric nanogenerators. *Advanced Materials*. 2016;**28**:98-105

[94] Liu LB, Yu Y, Yan C, Li K, Zheng ZJ. Wearable energy dense and power-dense supercapacitor yarns enabled by scalable graphene-metallic textile composite electrodes. *Nature Communications*. 2015;**6**:7260

[95] Rani S, Sharma Y. Fabrication of binder-free and high energy density yarn supercapacitor for wearable electronics. *IEEE Transactions on Power Electronics*. 2022;**37**:11

- [96] Pandit B et al. Two-dimensional hexagonal SNSE nanosheets as binder free electrode material for high-performance supercapacitors. *IEEE Transactions on Power Electronics*. 2020;**35**:11344
- [97] Sandhiya M, Balaji SS, Sathish M. Na<sub>2</sub>MoO<sub>4</sub>- incorporated polymer gel electrolyte for high energy density flexible supercapacitor. *ACS Applied Energy Materials*. 2020;**2**:11368
- [98] Elkholy AE, Dhmees AS, Heikal FET, Deyab MA. Mesoporous ZnMoS<sub>4</sub> as a supercapacitor electrode material with battery-like behavior. *New Journal of Chemistry*. 2019;**43**:1987-1992
- [99] Jain D, Kanungo J, Tripathi SK. Synergistic approach with redox additive for the development of environment benign hybrid supercapacitor. *Journal of the Electrochemical Society*. 2019;**166**:A3168-A3181
- [100] He N, Liao J, Zhao F, Gao W. Dual-core supercapacitor yarns: An enhanced performance consistency and linear power density. *ACS Applied Materials & Interfaces*. 2020;**12**:15211-15219
- [101] Shewale PS, Yun KS. NiCo<sub>2</sub>O<sub>4</sub>/RGO hybrid nanostructures on surface-modified Ni core for flexible wire-shaped supercapacitor. *Nanomaterials*. 2021;**11**:852
- [102] Li T, Wu Y, Wang Q, Zhang D, Zhang A, Miao M. TiO<sub>2</sub> crystalline structure and electrochemical performance in two-ply yarn CNT/TiO<sub>2</sub> asymmetric supercapacitors. *Journal of Materials Science*. 2017;**52**:7733
- [103] Zhao P et al. Iodine-steam functionalized reduced graphene oxide/oxidized carbon yarn electrodes for knittable fibriform supercapacitor. *Journal of Power Sources*. 2019;**442**
- [104] Zhao P et al. Three-dimensional ordered macroporous NiFe<sub>2</sub>O<sub>4</sub> coated carbon yarn for knittable fibriform supercapacitor. *Electrochimica Acta*. 2018;**281**:717-724